Determination of the electronic density in a medium by an inverse method based on double-Compton scattering in transmission imaging

Tuong Trong Truong, Maï K. Nguyen, Huy Duong Bui, Christian Daveau

DETERMINATION OF THE ELECTRONIC DENSITY IN A MEDIUM BY AN INVERSE METHOD BASED ON DOUBLE-COMPTON SCATTERING IN TRANSMISSION IMAGING.

T.T. Truong
Laboratoire de Physique Théorique et Modélisation.
Université de Cergy-Pontoise
Cergy-Pontoise. France
nguyen@ensea.fr

Mai K. Nguyen
Equipe Traitement des Images et du Signal
ENSEA/Université de Cergy-Pontoise
Cergy-Pontoise. France
tuong.truong@ptm.u-cergy.fr

H. D. Bui
Laboratoire de Mécanique des Solides.
Ecole Polytechnique
Palaiseau, France
bui@lms.palaiseau.fr

C. Daveau
Laboratoire de Mathématiques, Equipe d'Analyse numérique
Université Paris XI, Orsay
Orsay, France
Christian.Daveau@math.u-psud.fr

ABSTRACT

We propose a new method for reconstructing defects in bulk materials, via the recovery of the electronic volume density n_e in the material, using doubly Compton-scattered gamma photons in transmission imaging modality. We establish an integral relationship between the photon flux density after a double scattering and the product of electronic densities at two different sites. This photon flux density at different scattering angles can be measured by an energy-position detector in a fixed configuration. Thus the reconstruction of n_e can be formulated as an inverse problem of the integral relation, which is bilinear in the electronic densities. This theoretical result opens the way for a new imaging principle, which exploits scattered radiation rather than discarding it as in most existing imaging procedures. In this new procedure, the motion of the detector is no longer necessary as it is the case of conventional tomography.

NOMENCLATURE

$g(\mathbf{D}, \mathbf{S}\|\tau)$	: flux density at detection site $\mathbf{D}$ due to incoming pencil source beam having a trace at $\mathbf{S}$ on the detector.
$G(\mathbf{D}, \tau)$	: flux density at site $\mathbf{D}$ for given τ.
l	: distance slab-detector.
L	: thickness of slab.
$n_e(\mathbf{M})$	: electronic density at site $\mathbf{M}$. also noted $n_e(\mathbf{D}, \tau)$.
n_e^0, n_e^1	: constant electronic density in surrounding medium and in defect.
Φ_0	: constant incident flux density.
ρ	: distance $\|\mathbf{DS}\|$.
τ	: cotangent of the scattering angle θ.

INTRODUCTION

The goal in non-destructive control is to obtain information (location, form, representative parameters) about defects in bulk materials. This is up to now done by X-ray or gamma ray transmission imaging. In these methods of investigation, the defect is represented by its linear attenuation distribution μ. The data consists of line integrals of the attenuation density along lines joining source points to detector points. A three dimensional reconstruction of the volume defect can be realized if a complete set of data is obtained with various directions of the incident source beam. However this may not be always realizable in practical situations where the geometry of the piece of material imposes severe restrictions on the motion of the radiation source.

In this paper, we describe an alternative method of investigation of defects. Instead of representing the material under study by its absorption function, as usually done, we shall describe it alternatively by its electronic density n_e. Indeed at the location of defects (inclusions, voids or cracks) n_e will change drastically and will exhibit discontinuous jumps in values. The distribution of scattered photons will change accordingly. The determination of n_e from single scattered photons (in-

stead of non-scattered ones) has been introduced in Compton Scatter Tomography [6]. But no analytical inversion procedure is available. In the present work we propose an analytical inversion method for obtaining n_e from the series of doubly Compton-scattered photon distributions *at various scattering angles*. Moreover we show that in this procedure the motion of the detector is no longer necessary and consequently may be more interesting from the point of view of operational level [2, 3].

In order to focus solely on the scattering aspect, the attenuation mainly due to photoelectric effect shall be neglected here. This hypothesis is acceptable in the low energy range of gamma photons. In a transmission imaging system with collimated detector, if the material slab is of thickness L and limited by parallel planes, for incoming gamma photons perpendicularly to the slab to emerge parallel to the incident direction, there must be at least two Compton collisions. This is why we propose to exploit the properties of double Compton scattering for determining n_e, since higher order collisions have much weaker probability of occurrence.

The paper is organized as follows. In the next section, we establish the basic relation connecting the flux density of photons $G(\mathbf{D}, \tau)$ - image measured on the detector plane - to $n_e(\mathbf{r})$ - the electronic distribution in the bulk material. This relation will be called also the *"imaging equation"*. Next, we introduce the concept of *Transmission Pencil Source Function* (TPSF), which plays the role of the well-known PSF in emission imaging. Then images of cracks of simple form are computed as illustrations with the use of the TPSF. In the following section, the *inverse problem* of determining the volume extent of the crack using the measured flux density $G(\mathbf{D}, \tau)$, is considered. It is shown that an *analytical* solution exists if one makes use of the whole *set of data collected at all scattering angles* θ. This theoretical result opens the way for a new transmission imaging principle in which one takes advantage of the double Compton scattering whereby the complete data is obtained without moving the detector. Conclusions and outlook are given in the last section.

IMAGING EQUATION

We consider an incident gamma-ray beam of initial energy E_0 and of constant flux density Φ_0 on a slab of material of thickness L, in which the electronic density is $n_e(\mathbf{r})$. Normally the gamma rays at this energy will go through the object, if no attenuation is assumed. They are collected on the plane of a collimated gamma camera, which has an axis parallel to the incident beam, and located at a distance l from the slab face.

However part of the gamma rays will undergo

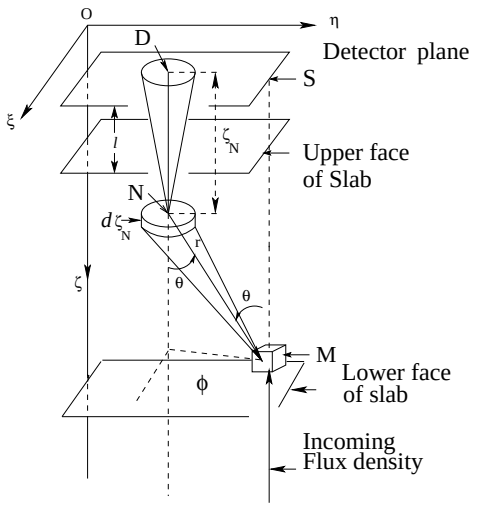

Figure 1: Schematic representation of the functioning principle

Compton scattering, and actually two scattering if they are to emerge parallel to the incident direction (see figure 1). They form images *parameterized by the scattering angle* θ, or alternatively by the outgoing photon energy E. The photon energy recorded after two collisions with the same scattering angle θ is given by the Compton formula:

$$E = \frac{E_0}{1 + 2\epsilon(1 - \cos\theta)},$$

where $\epsilon = \frac{E_0}{mc^2}$ is the ratio of the initial photon energy to the rest energy of the electron. This formula has the same form as the formula for one collision, but with 2ϵ instead of ϵ.

Let Φ_0 be the constant incident flux density. Now the flux density of photons $\Phi(\mathbf{M})$, scattered at a site $\mathbf{M}\,(\xi_M, \eta_M, \zeta_M)$ (first collision site) in the bulk material into a solid angle $d\Omega_N$ is given by the expression:

$$\Phi_0 r_e^2 P(\theta) d\Omega_N n_e(\mathbf{M}) d\mathbf{M} = \Phi(M) d\sigma_N$$

where $d\Omega_N = d\sigma_N / MN^2$, $d\sigma_N$ being the elementary surface subtended at site $\mathbf{N}\,(\xi_N, \eta_N, \zeta_N)$(second collision site). The differential Compton cross section is the term $r_e^2 P(\theta)$ where r_e is the classical electron radius and $P(\theta)$, the so-called Klein-Nishina probability function [1].

$$P(\theta) = \frac{1}{2[1 + \varepsilon(1 - \cos\theta)]^2}$$
$$\left[1 + \cos^2\theta + \frac{\varepsilon^2(1 - \cos\theta)^2}{1 + \varepsilon(1 - \cos\theta)}\right]. \qquad (1)$$

The flux density of photons arriving at site $\mathbf{N}$ is then obtained by dividing out $d\sigma_N$. This flux will be scattered next at site $\mathbf{N}$ into the solid angle $d\Omega_D$. Finally the flux density photons collected at detection site $\mathbf{D}$ $((\xi_D, \eta_D, 0)$ reads:

$$\Phi_0 r_e^2 P(\theta) \frac{n_e(\mathbf{M})}{MN^2} d\mathbf{M} r_e^2 P(\theta) \frac{n_e(\mathbf{N})}{ND^2} d\mathbf{N}.$$

In figure 1, we have given also the coordinate system to be used in the calculations to come. The scattering site $\mathbf{M}$ has coordinates:

$$\begin{aligned} \xi_M &= \xi_D + r\sin\theta'\cos\phi, \\ \eta_M &= \eta_D + r\sin\theta'\sin\phi, \\ \zeta_M &= \zeta_N + r\cos\theta'. \end{aligned}$$

where (r, θ', ϕ) are the local spherical coordinates centered at $\mathbf{N}$.

The total flux density $G(\mathbf{D}, \tau)$ on the detector is the summation on contributions of:

• for given $\mathbf{N}$, all sites $\mathbf{M}$ in the medium on a cone of apex $\mathbf{N}$, opening angle θ and axis $O\zeta$,

• all sites $\mathbf{N}$ on a vertical at site $\mathbf{D}$, verifying $l < \zeta_N < \infty$, since the slab is put at a distance l from the detector.

Thus we introduce the corresponding integration measures:

$$\begin{aligned} \delta(Cone) &= r^{-1}\delta(\theta' - \theta) \\ \delta(Line) &= \delta(\xi_N - \xi_D)\delta(\eta_N - \eta_D). \end{aligned}$$

Consequently the photon flux density at $\mathbf{D}$ is given by:

$$G(\mathbf{D}, \tau) = [r_e^2 P(\theta)]^2 \int_l^\infty \delta(Line)\, d\xi_N d\eta_N d\zeta_N$$

$$\int \frac{1}{r}\delta(\theta' - \theta) r^2 dr d\theta' \sin\theta' d\phi \frac{1}{r^2} n_e(\mathbf{M}) \frac{1}{\zeta^2} n_e(\mathbf{N}) \Phi_0. \tag{2}$$

(Recall that Φ_0 is the incident flux density of photons.)

Some integrations are now performed in order to eliminate the δ-functions. The result may be expressed in terms of the constant:

$$K(\tau) = [r_e^2 P(\theta)]^2 \sin\theta.$$

where $\tau = \cot\theta$ and reads as:

$$\frac{G(\mathbf{D}, \tau)}{K(\tau)} = \int_l^\infty \frac{d\zeta_N}{\zeta_N^2} n_e(\mathbf{D}, \zeta_N) \int_{0_+}^\infty \frac{dr}{r} \int_0^{2\pi} d\phi$$

$$n_e(\xi_D + r\sin\theta\cos\phi, \eta_D + r\sin\theta\sin\phi, \zeta_N + \cos\theta)\Phi_0.$$

Introducing now the projection of site $\mathbf{M}$ on the detector plane $\mathbf{S}$, we observe that $\xi_S = \xi_D + r\sin\theta\cos\phi$, $\eta_S = \eta_D + r\sin\theta\sin\phi$ and $\zeta_S = 0$. We may put the result as:

$$G(\mathbf{D}, \tau) = K(\tau) \int_{0_+}^\infty \frac{dr}{r} \int_0^{2\pi} d\phi$$

$$\int_l^\infty \frac{d\zeta_N}{\zeta_N^2} n_e(\mathbf{D}, \zeta_N) n_e(\mathbf{S}, \zeta_N + r\cos\theta)\Phi_0, \tag{3}$$

here this expression is evidently bilinear in the electron densities. Let us call $\rho = r\sin\theta$, the distance between sites $\mathbf{D}$ and $\mathbf{S}$, i.e. $|\mathbf{D} - \mathbf{S}| = \rho$, then we can rewrite conveniently this expression as:

$$G(\mathbf{D}, \tau) = K(\tau) \int_{0_+}^\infty \frac{\rho d\rho}{\rho^2} \int_0^{2\pi} d\phi$$

$$\int_l^\infty \frac{d\zeta_N}{\zeta_N^2} n_e(\mathbf{D}, \zeta_N) n_e(\mathbf{S}, \zeta_N + \rho\tau)\Phi_0,$$

this can be rearranged as an integral over $\mathbf{S}$ as:

$$G(\mathbf{D}, \tau) = \int_{beamsection} d\mathbf{S} g(\mathbf{S}, \mathbf{D}|\tau)\Phi_0, \tag{4}$$

where $g(\mathbf{S}, \mathbf{D}|\tau)$, is defined as *the Transmission Pencil Source Function* (TPSF) of the problem. *The TPSF represents the transmission image by double Compton scattering of a unit flux density pencil source at infinity incoming normally on the detector plane.* This function will play the role of the PSF function in emission imaging. It is given by:

$$g(\mathbf{S}, \mathbf{D}|\tau) = \frac{K(\tau)}{\rho^2} \int_l^\infty \frac{d\zeta_N}{\zeta_N^2} n_e(\mathbf{D}, \zeta_N) n_e(\mathbf{S}, \zeta_M). \tag{5}$$

where $\zeta_M = (\zeta_N + \rho\tau)$. This function describes thus the illumination of the material slab by an incoming pencil beam and serves to explore the structure of defects in the bulk.

For an arbitrary incoming beam with finite section, e.g. from an extended source far away, $\phi_0 = \phi_0(\mathbf{S})$ and this must be taken care of in the integration standing in equation (4).

IMAGES OF SIMPLE SYSTEMS

The purpose of this section is to illustrate the imaging mechanism of the TPSF on simple systems. As already mentioned, gamma rays can be used to reconstruct variations of the electronic density at very small (atomic) scales. But for the localization of macroscopic defects in materials, these details are irrelevant and homogeneous medium can be considered to have a constant electronic density equal to its mean macroscopic value [4]. Defects may appear as cracks or voids where the electronic density drops brutally to zero or filled volumes with a different value of the electronic density. And this is precisely what we wish to detect.

1-Image of a homogeneous material slab

As the electronic density is assumed to be constant and equal to n_e^0, the TPSF can be explicitly

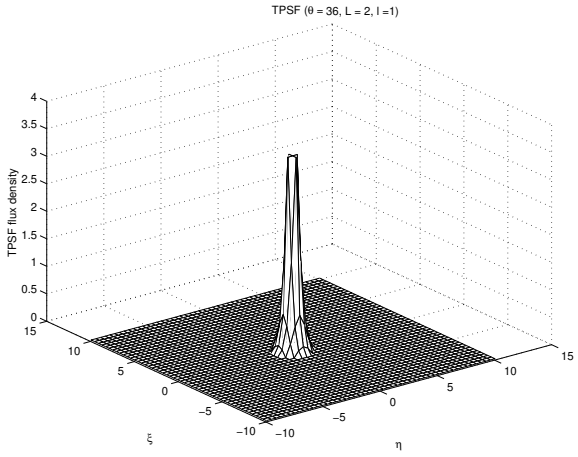

Figure 2: TPSF Flux density at $\theta = 36$ degrees

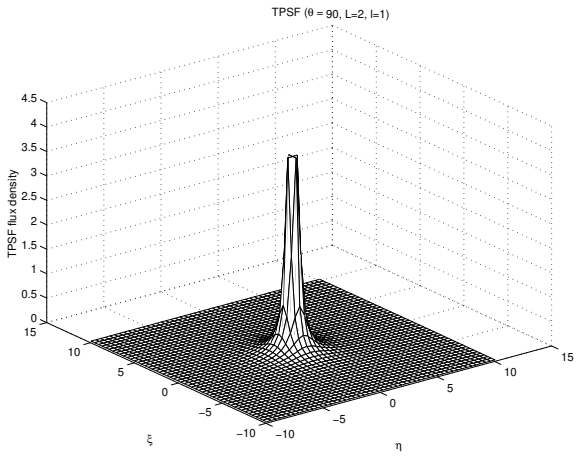

Figure 3: TPSF Flux density at $\theta = 90$ degrees

evaluated:

$$\frac{g(\mathbf{S},\mathbf{D}|\tau)}{K(\tau)(\frac{n_e^0}{\rho})^2} = \begin{cases} Y(L-\rho\tau)\frac{(L-\rho\tau)}{l(l+L-\rho\tau)} & \text{if } \tau > 0 \\ Y(L+\rho\tau)\frac{(L+l+\rho\tau)}{(l+L)(-\rho\tau)} & \text{if } \tau < 0 \\ \frac{L}{l(l+L)} & \text{if } \tau = 0. \end{cases} \quad (6)$$

Here $Y(x)$ stands for the Heaviside unit step function. Rotational symmetry around the incident pencil beam is reflected by the sole dependence on ρ. This image will serve as basis for detecting defects. Fig 2 and Fig.3 give a representation of the TPSF at two scattering angles.

At 90 degrees scattering angle, the TPSF has a very simple behavior, i.e. its varies as ρ^{-2}.

Finally the form of the peak changes according to the ratio l/L.

2-Image of a linear defect

Consider a linear defect situated on a line perpendicular to the detector plane at a site $\mathbf{S}_0$ on the detector plane. The defect has a length $h << L$ and its middle point is at a distance ζ_0 from $\mathbf{S}_0$. On the defect there is an electronic density n_e^1, different from the slab electronic density n_e^0 . The question is now how would the TPSF detect this defect? Two situations are possible:

• if the defect is not exactly positioned on the direction of the incoming beam and the detection site $\mathbf{D}$ different from $\mathbf{S}_0$, then the measured flux density $g(\mathbf{S},\mathbf{D}|\tau)$ is the same as in the case of the homogeneous slab (see equation 6). But if $\mathbf{D}$ is precisely at $\mathbf{S}_0$ then the measured flux density is, for $\tau > 0$, given by:

$$g(\mathbf{S},\mathbf{D}|\tau) = \frac{K(\tau)}{\rho_0^2}$$

$$\left\{ \frac{(n_e^0)^2(L-\rho_0\tau)}{l(l+L-\rho_0\tau)} - \frac{[(n_e^0)^2-(n_e^1)^2]h}{\zeta_0^2 - \frac{1}{4}h^2} \right\}, \quad (7)$$

where $\rho_0 = |\mathbf{S}_0\mathbf{D}|$. When $n_e^1 \to 0$, the defect becomes a crack, and when $h \to 0$ we get the limit of the point defect. Then it is clear that the TPSF cannot "see" a point defect since we recover the flux density of equation 6.

• if the probing pencil beam falls directly on the defect, then one would measure, also for $\tau > 0$ or the scattering angle $0 < \theta < \pi/2$:

$$g(\mathbf{S},\mathbf{D}|\tau) = \frac{K(\tau)}{\rho^2}$$

$$\left\{ \frac{(n_e^0)^2(L-\rho\tau)}{l(l+L-\rho\tau)} - \frac{[(n_e^0)^2-(n_e^1)^2]h}{(\zeta_0-\rho\tau)^2 - \frac{1}{4}h^2} \right\}. \quad (8)$$

Thus a linear vertical defect would cause a jump in the recorded flux density as compared to the pattern of a homogeneous slab. For $\tau < 0$ or a scattering angle larger than $\pi/2$, the main features of the pictures remains the same but the expressions are slightly modified.

3-Image of a rectangular defect

Having studied in detail the case of a linear perpendicular defect in the previous section, it is now easy to treat many other cases. The simplest one which can be generated is the case of the rectangle perpendicular to the detector with center at (ρ_0, ζ_0), with sides (h', h) respectively parallel and orthogonal to the detector.

• Despite the non-zero width h', the behavior of the TPSF with respect to this kind of defect is exactly the same as in the case of the linear defect of the previous subsection, if the incident pencil beam does not cross the defect and if the detection line (the line perpendicular to the detector at $\mathbf{D}$)

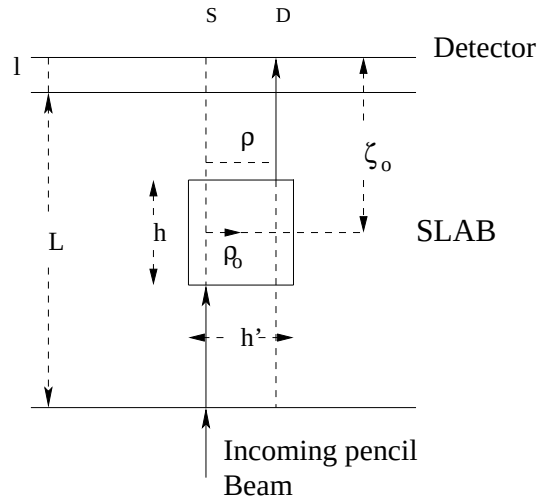

Figure 4: Rectangular defect plane with **S** and **D** inside the plane.

crosses the defect. To see the spread of the defect parallel to the detector one should move **D** along the detector plane so that $(\rho_0 - h'/2) < \rho < (\rho_0 + h'/2)$.

• The interesting case occurs when the lines perpendicular to the detector at **S** and at **D** are inside the rectangle and at a distance $\rho < h'$.

Then there are two values of the flux density depending on τ :

a) if $\rho\tau \leq h$ and $\rho < h'$ we have:

$$g(\mathbf{S},\mathbf{D}|\tau) = \frac{K(\tau)}{\rho^2}\,\{$$

$$2n_e^0 n_e^1\left(\frac{(\zeta_0-\rho\tau)}{(\zeta_0-\rho\tau)^2-\frac{1}{4}h^2}-\frac{\zeta_0}{\zeta_0^2-\frac{1}{4}h^2}\right)+$$

$$(n_e^1)^2\left(\frac{(h-\rho\tau)}{(\zeta_0-\frac{1}{2}h)(\zeta_0-\rho\tau+\frac{1}{2}h)}+\right.$$

$$\left.(n_e^0)^2\left(\frac{(L-\rho\tau)}{l(l+L-\rho\tau)}-\frac{(h+\rho\tau)}{(\zeta_0+\frac{1}{2}h)(\zeta_0-\rho\tau-\frac{1}{2}h)}\right)\right\}$$

b) but if $\rho\tau > h$ and $\rho < h'$ we have:

$$g(\mathbf{S},\mathbf{D}|\tau) = \frac{K(\tau)}{\rho^2}\left\{(n_e^0)^2\left(\frac{(L-\rho\tau)}{l(l+L-\rho\tau)}\right.\right.$$

$$\left.-\frac{h}{(\zeta_0-\rho\tau)^2-\frac{1}{4}h^2}-\frac{h}{\zeta_0^2-\frac{1}{4}h^2}\right)$$

$$\left.+n_e^0 n_e^1\left(\frac{h}{(\zeta_0-\rho\tau)^2-\frac{1}{4}h^2}+\frac{h}{\zeta_0^2-\frac{1}{4}h^2}\right)\right\} \qquad (9)$$

From these results one can draw several conclusions:

- for $h \to 0$, we get the limit of an infinitely thin horizontal defect: the flux density is that of the homogeneous medium, in other words it is "invisible" by the TPSF. Also it is easy to generalize to a horizontal disk defect or to any horizontal planar defect: they cannot be detected by the TPSF.
- for $n_e^1 \to 0$, we get the limit of a rectangular crack. This crack does present a non-zero "thickness" h with respect to the direction of the incoming probing radiation.
- There are similar results for $\tau < 0$.

4-Image of an arbitrary defect

From the previous considerations, we can make general observations on how images are formed by the TPSF. First of all, it must present a certain "thickness" with respect to the incoming pencil radiation. Then we can decompose the problem into planar imaging problem by considering the intersection of the plane (π) which contains the two parallel lines perpendicular to the detector at **D** and at **S** and the the slab of material to be investigated.

If these lines do not intersect the section of a defect (Σ) in (π), then the flux density recorded on the detector is that of a homogeneous medium. Now if the perpendicular line at **D** intersects (Σ), then the measured flux density has the pattern of a linear perpendicular defect studied in the previous subsection. Note that the height of such a defect varies as site **D** moves on the detector plane, and in the previous subsection we have looked at a particular section (Σ), which is a simple rectangle. Of course, the interesting case would be the case where both perpendicular lines at **D** and **S** intersect (Σ), but this times the intersection lengths are no longer equal. The general effect remains similar.

So in principle, a general image obtained of an arbitrary defect of nonzero measure in the vertical direction by the TPSF, can be constructed from the TPSF image of a finite linear perpendicular defect. The question is now how the defect in the bulk can be reconstructed in space when a set of images, labelled by τ, or equivalently by the scattering angle θ has been collected beforehand.

THE INVERSE PROBLEM

This is the problem of reconstructing the electronic density $n_e(\mathbf{r})$ from measurements made on the detector. In this section, we show that this problem has a solution, provided that certain working conditions are assumed. More precisely, we show that the TPSF images can be used effectively to reconstruct the electronic density as follows.

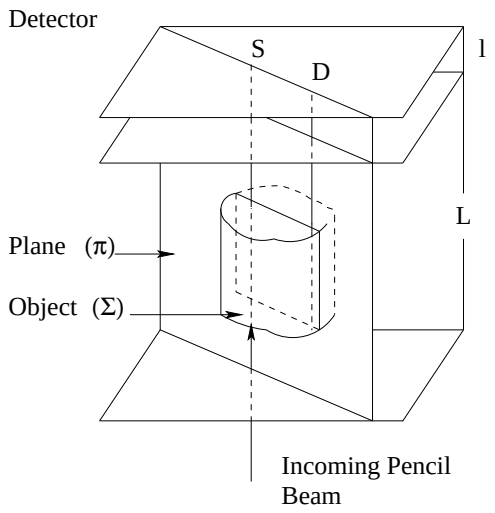

Figure 5: Arbitrary object analysis

Introducing the one-dimensional Fourier representation of the electronic densities:

$$n_e(\mathbf{D},\zeta_N) = \int_{-\infty}^{\infty} dw\, e^{2i\pi w\zeta_N}\, \tilde{n}_e(\mathbf{D},w),$$

$$n_e(\mathbf{S},\zeta) = \int_{-\infty}^{\infty} dw'\, e^{2i\pi w'\zeta}\, \tilde{n}_e(\mathbf{S},w'),$$

in equation (5), the TPSF can be recast under the form:

$$g(\mathbf{S},\mathbf{D}|\tau) = \frac{K(\tau)}{\rho^2} \int\int dw\, dw'\, \tilde{n}_e(\mathbf{D},w)\, \tilde{n}_e(\mathbf{S},w')$$

$$\mathcal{J}_l(w+w')\, \exp[2i\pi(lw + lw' + w'\rho\tau)], \qquad (10)$$

where:

$$\mathcal{J}_l(w) = \int_l^{\infty} \frac{d\zeta_N}{\zeta_N^2}\, e^{2i\pi(w+w')\zeta_N} = 2i\pi w$$

$$\{e^{2i\pi lw}\, [Ci(2\pi l|w|) - i\,\varepsilon(w)\, Si(2\pi l|w|)] - \frac{i}{2\pi wl}\},$$

$\varepsilon(w)$ being the sign function of w [5]. Now since $\tau \in \mathcal{R}$, we could use it as Fourier variable to invert equation 10, and obtain:

$$\int_{-\infty}^{\infty} d\tau\, e^{-2i\pi\nu\tau}\, \frac{g(\mathbf{S},\mathbf{D}|\tau)}{K(\tau)} = \frac{1}{\rho^2}\, \tilde{n}_e(\mathbf{S},\frac{\nu}{\rho}) e^{2i\pi l\frac{\nu}{\rho}}$$

$$\int_{-\infty}^{\infty} dw\, \tilde{n}_e(\mathbf{D},w)\, \mathcal{J}_l(w+\frac{\nu}{\rho}) e^{2i\pi lw}.$$

Here the left hand side appears as *a superposition of TPSF images taken at various scattering angles*, however the right hand side remains a bilinear construct in the electronic densities at two different sites. To get a better insight, we transform the right hand side by back Fourier transform into:

$$\int_{-\infty}^{\infty} dw\, \tilde{n}_e(\mathbf{D},w)\, \mathcal{J}_l(w+\frac{\nu}{\rho}) e^{2i\pi lw} =$$

$$\int_l^{\infty} \frac{d\zeta}{\zeta^2} n_e(\mathbf{D},\zeta) e^{2i\pi\frac{\nu}{\rho}(\zeta-l)},$$

and end up, after another Fourier inversion with a final form:

$$\int_{-\infty}^{\infty} d\tau\, e^{-2i\pi\nu\tau}\, \frac{g(\mathbf{S},\mathbf{D}|\tau)}{K(\tau)} =$$

$$\frac{1}{\rho^2}\, \tilde{n}_e(\mathbf{S},\frac{\nu}{\rho}) \int_l^{\infty} \frac{d\zeta}{\zeta^2} n_e(\mathbf{D},\zeta)\, e^{2i\pi\frac{\nu}{\rho}\zeta}. \qquad (11)$$

Remark. One could exchange the roles of $\mathbf{D}$ and $\mathbf{S}$: the incoming pencil beam falls perpendicularly on the detector at site $\mathbf{D}$ and $\mathbf{S}$ becomes the detection site. Then one has, with the same separation ρ:

$$\int_{-\infty}^{\infty} d\tau\, e^{-2i\pi\nu\tau}\, \frac{g(\mathbf{D},\mathbf{S}|\tau)}{K(\tau)} =$$

$$\frac{1}{\rho^2}\, \tilde{n}_e(\mathbf{D},\frac{\nu}{\rho}) \int_l^{\infty} \frac{d\zeta}{\zeta^2} n_e(\mathbf{S},\zeta)\, e^{2i\pi\frac{\nu}{\rho}\zeta}.$$

Inversion is in fact based on one of these equations. In general, we have thus a pair of integral equations which are quadratic in the unknown functions $n_e(\mathbf{r})$. To our knowledge a general solution does not exist. However under certain practical hypotheses, an inversion procedure may be constructed.

Let us consider equation (11), which describes the imaging of the medium by the TPSF centered at $\mathbf{S}$, the measurement of flux density being made at site $\mathbf{D}$. If $\mathbf{S}$ is chosen in such a way that $\tilde{n}_e(\mathbf{S},\frac{\nu}{\rho})$ is *known*, one may locate in the sample a vertical line to the detector along which the material is homogeneous, i.e. free of defects. Then we have:

$$n_e(\mathbf{S},\zeta) = \begin{cases} n_e^0 & \text{if } l < \zeta < (L+l) \\ 0 & \text{otherwise.} \end{cases}$$

Then $\tilde{n}_e(\mathbf{S},\frac{\nu}{\rho})$ may be exactly evaluated:

$$\tilde{n}_e(\mathbf{S},\frac{\nu}{\rho}) = \frac{n_e^0\rho}{\pi\nu}\, e^{-i\pi\frac{\nu}{\rho}(2l+L)}\, \sin\pi\frac{\nu}{\rho}L.$$

Hence

$$\int_l^{\infty} \frac{d\zeta}{\zeta^2} n_e(\mathbf{D},\zeta)\, e^{2i\pi\frac{\nu}{\rho}\zeta} = \frac{\pi\nu\rho}{n_e^0}$$

$$\frac{e^{i\pi\frac{\nu}{\rho}(2l+L)}}{\sin\pi\frac{\nu}{\rho}L} \int_{-\infty}^{\infty} d\tau\, e^{-2i\pi\nu\tau}\, \frac{g(\mathbf{S},\mathbf{D}|\tau)}{K(\tau)}. \qquad (12)$$

To extract now the electronic density at **D**, we perform inverse Fourier transformation by multiplying equation (12) on both sides by

$$\int_{-\infty}^{\infty} d(\frac{\nu}{\rho})\, e^{2i\pi\frac{\nu}{\rho}\zeta'},$$

and integrate over $(\frac{\nu}{\rho})$ to get the expression of the electronic density at site $(\mathbf{D}, \zeta')$:

$$n_e(\mathbf{D},\zeta') = \zeta'^2 \int_{-\infty}^{\infty} d(\frac{\nu}{\rho})\, e^{2i\pi\frac{\nu}{\rho}(\frac{2l+L}{2}-\zeta')}\, \frac{\pi\nu\rho}{n_e^0}$$

$$\frac{1}{\sin\pi\frac{\nu}{\rho}L} \int_{-\infty}^{\infty} d\tau\, e^{-2i\pi\nu\tau}\, \frac{g(\mathbf{D},\mathbf{S}|\tau)}{K(\tau)}. \qquad (13)$$

An alternative way of inverting consists of choosing a fixed detection site **D** with a perpendicular line along which the electronic density is constant. Then one can calculate immediately:

$$\int_{l}^{\infty} \frac{d\zeta}{\zeta^2} n_e(\mathbf{D},\zeta)\, e^{2i\pi\frac{\nu}{\rho}\zeta} = n_e^0 \mathcal{J}_l(\frac{\nu}{\rho}).$$

Hence one deduces the Fourier transform $\tilde{n}_e(\mathbf{S}, \frac{\nu}{\rho})$ of $n_e(\mathbf{S}, \tau)$ and consequently:

$$n_e(\mathbf{S},\zeta') = \int_{-\infty}^{\infty} d(\frac{\nu}{\rho})\, e^{2i\pi\frac{\nu}{\rho}\zeta'}$$

$$\frac{\rho^2}{n_e^0 \mathcal{J}_l(\frac{\nu}{\rho})} \int_{-\infty}^{\infty} d\tau\, e^{-2i\pi\nu\tau}\, \frac{g(\mathbf{D},\mathbf{S}|\tau)}{K(\tau)}. \qquad (14)$$

This time we keep the detection site fixed, and move around the incoming pencil beam to collect the data before computing the reconstruction of the defect. This is an equivalent procedure and the choice between the two may depend on the practicability of the measures at hand.

CONCLUSIONS AND OUTLOOK

In this work, we propose an *analytical* inverse method to determine the electronic density from double Compton scattering in transmission imaging. This result is used for the detection of defects in homogeneous medium. This detection procedure does not require the motion of neither the incident radiation source nor the material under investigation. This represents a real advantage in some non-destructive controls in which the number of views in conventional tomography is very limited.

References

[1] H. H. Barrett and W. Swindell, *Radiological Imaging* I and II, Academic Press, New York, (1981).

[2] Mai K. Nguyen, C. Fay, L. Eglin and T. T. Truong, Apparent image formation by Compton scattered photons in gamma-ray imaging *IEEE Signal Processing Letters*, **8** (9), pp. 248-251, 2001.

[3] Mai K. Nguyen and T. T. Truong, On an integral transform and its inverse in nuclear imaging, *Inverse Problems*, **18** (1), pp. 265-277, 2002.

[4] R. Cesaro, A.L. Hanson, G.E. Gigante, L.J. Pedraza and S.Q.G. Mathtaboally, *Interactions of keV Photons with Matter and New Applications*, Physics Reports **213** (3), pp. 117-178, 1992.

[5] J. Lavoine, *Transformation de Fourier des Pseudo-fonctions avec Tables de Nouvelles Transformées* , CNRS, Paris, (1963).

[6] E. M. A. Hussein, Compton Scatter Imaging Systems, in *Bioinstrumentation: research, developments and applications*, D. L. Wise Editor, chap.35, pp. 1053-1086, 1990.